EMC Chamber Quiet Zone Qualification for Applications Above 1 GHz Using Frequency Domain Mode Filtering

Zhong Chen, *Member, IEEE*, and Stuart F. Gregson

***Abstract*— Anechoic chambers used for electromagnetic compatibility (EMC) measurements above 1 GHz are qualified based on the site voltage standing wave ratio (SVSWR) method as per the international standard CISPR 16-1-4. With one antenna at the fixed position, some distance away from the quiet zone (QZ), the SVSWR is acquired by moving a dipole-like antenna along several linear paths that are located at the edge of the QZ. To reduce test burden, the SVSWR method under-samples the measurement by design, in that only six discrete points along each 40 cm linear travel path are measured. As a result, the test results are generally overly optimistic. In this article, we propose to use a novel cylindrical mode coefficient (CMC)-based frequency domain mode filtering techniques to obtain the VSWR. Here, we measure the vector pattern cut of the dipole-like test antenna with an offset placement at the outer edge of QZ. The antenna is then mathematically translated to the rotation center, whereupon a bandpass filter that tightly encloses the test antenna mode spectrum is applied. Two approaches are studied herein for translating the rotation center. One is by applying a path length correction to both magnitude and phase, and the other is by performing a cylindrical far-field transformation on the quasi-far-field data. The difference between the mode filtered antenna pattern and the original perturbed pattern is used to derive the chamber SVSWR. In contrast to the conventional technique, the proposed, novel method does not suffer from positional under-sampling, so it is well-placed to be applied at microwave frequencies and above.**

***Index Terms*— Cylindrical mode coefficient (CMC), electromagnetic compatibility (EMC) site validation, mode filtering, range multipath evaluation, site voltage standing wave ratio (SVSWR).**

I. Introduction

SITE voltage standing wave ratio (SVSWR) is used as a metric to qualify the performance of anechoic chambers used for electromagnetic compatibility (EMC) testing at frequencies above 1 GHz [1]. SVSWR is one of the most important parameters to judge whether a chamber is permitted to be used for conducting compliant EMC measurements. However, the existing method is known to be lacking repeatability, as has been reported by several researchers [2]–[4]. A typical SVSWR test configuration is shown in Fig. 1. A dipole-like omni-directional antenna is placed at various locations in the quiet zone (QZ), such as at the front (F), left (L), or right (R) locations. The remote source antenna (RSA), which is typically a broadband ridged waveguide horn, is located some distance away (usually 3 m from the front edge of the QZ) and is boresighted to the center of the QZ. The omni-directional antenna is used to sample the standing wave along several 40 cm linear paths, each consisting of six discrete test points (at 0, 2, 10, 18, 30, and 40 cm away from the first position). As documented [2], [3], the six discrete points are chosen as a compromise to save test time. These irregularly spaced test points are attempts at breaking up possible harmonics. Nonetheless, they severely under-sample the standing wave, and the resulting VSWR is characteristically less stringent.

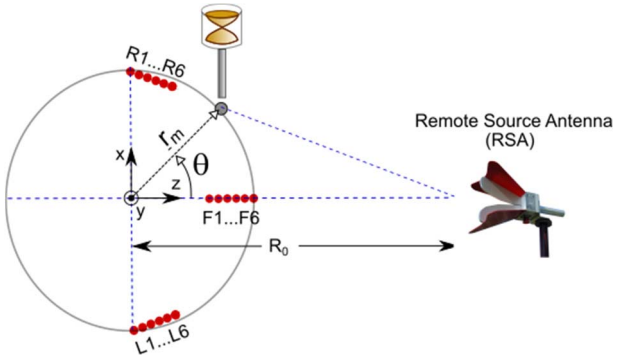

Fig. 1. SVSWR test setup per CISPR 16-1-4.

To overcome the under-sampling difficulties, time domain techniques were developed [5] in recent years, which resulted in the publication of the American national standard C63.25.1 [16]. The limitation of the time domain method is that it requires broadband antennas that possess a short ring-down time in order to achieve the necessary resolution. Many of the practical antennas cannot satisfy this condition. In [6], a different technique was proposed which consisted of performing several single pattern-cut measurements with the omni-directional antenna set at the edge of the QZ. The resulting pattern is then compared with numerical simulations reconstructed from the antenna's spherical mode coefficients (SMCs) to derive the SVSWR ripple size. The difference in dB between the raw pattern to the reference data is the

Manuscript received May 14, 2021; revised September 8, 2021; accepted September 9, 2021. Date of publication October 8, 2021; date of current version October 19, 2021. The Associate Editor coordinating the review process was Kristen M. Donnell. *(Corresponding author: Zhong Chen.)*

Zhong Chen is with ETS-Lindgren Inc., Cedar Park, TX 78613 USA (e-mail: zhong.chen@ets-lindgren.com).

Stuart F. Gregson is with Next Phase Measurements, Garden Grove, CA 92841 USA (e-mail: stuart.gregson@npmeas.com).

Digital Object Identifier 10.1109/TIM.2021.3119143

chamber SVSWR. The method is attractive in that the setup and measurement processes are rather simple. The antenna is rotated by the turntable, which is readily available in any EMC chamber. There is no need to under-sample the antenna pattern by taking a sparse angular step, as the measurement can be easily automated. However, one drawback is that the results and accuracy depend on *a priori* knowledge of the antenna pattern. This could be onerous due to the fact that the antenna must be numerically modeled or calibrated beforehand which increases the burden on the experimentalist.

This article is an extension of [7]. In this study, we take a notably different approach to obtain the reference antenna pattern by applying the far-field cylindrical mode filtering technique [8], [9]. In [9], it has been shown that this is an effective measurement and post processing technique that can be used to correct far-field antenna pattern data, where only a single polarized great circle pattern cut is taken. The existing site qualification standards [1], [2] are based on sampling the voltage standing wave at several points on the periphery of the QZ. This is convenient for the mode filtering technique, as the intentional offset from the QZ center provides a natural advantage for the mode filtering technique to remove the chamber reflections and to obtain the reference pattern. In the proposed approach, a single cut pattern dataset with the antenna at the offset position is collected. The antenna pattern is then mathematically translated back to its rotation center, after which, the antenna cylindrical mode coefficients (CMCs) are computed. The cylindrical modes associated with the measurement antenna are now confined to the lower orders encompassing just the antenna, rather than the much larger QZ radius. Meanwhile, the modes associated with the chamber multipath effects do not get translated coherently and remain spread to the higher-order modes. This provides a separation between the antenna modes and modes associated with the range multipath. The underlying antenna pattern can therefore be filtered and extracted with minimal impact from the chamber. No *a priori* knowledge of the antenna pattern, auxiliary measurements, or computational electromagnetic (CEM) simulations is needed. The SVSWR measurement process is thus reduced to performing several 1-D pattern cuts. Fig. 1 shows a typical test configuration, also shown are the test points (e.g., L1, . . . ,L6, F1, . . . ,F6, and R1, . . . ,R6) in a traditional SVSWR measurement. As is proposed in [6], we recommend to collect three pattern cuts, as shown in Fig. 2, i.e., one with antennas vertical polarized and two with antenna horizontal polarized but orthogonally oriented. In both horizontal cases, the RSA should be oriented identically (i.e., horizontally polarized). The two horizontal orientations of the test antenna complement the patterns of each other to reduce effects from the nulls of the dipole-like antennas.

Figs. 3 and 4 show different views of the test setup including a view depicting the offset biconical test antenna in the chamber. Here, the receive antenna was an ETS-Lindgren Model 3117 double-ridged waveguide horn whilst the test antenna was an ETS-Lindgren Model 3183B end-fed mini-biconical antenna. Both instruments operate from 1 to 18 GHz. The mini-biconical test antenna is specifically designed to meet the pattern requirements in CISPR 16-1-4 [1] and ANSI C63.25.1 [16] (to be sufficiently dipole-like across the entire frequency band) for chamber validation testing.

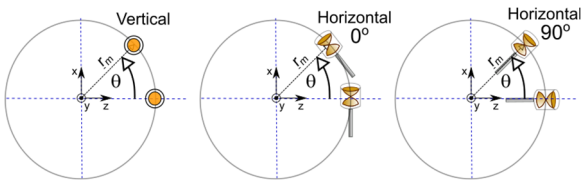

Fig. 2. Three pattern cuts to qualify an EMC chamber.

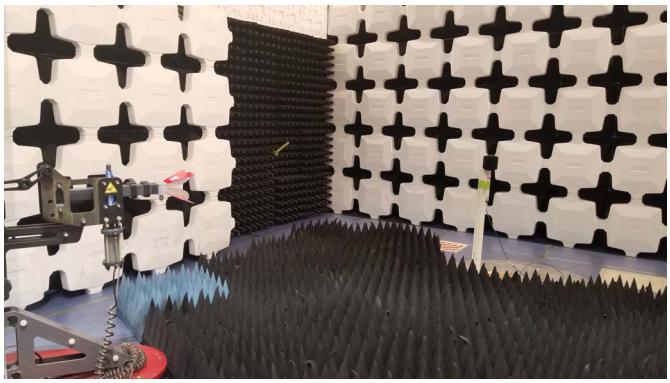

Fig. 3. Test setup showing EMC chamber with the RSA seen to the left and the biconical to the right.

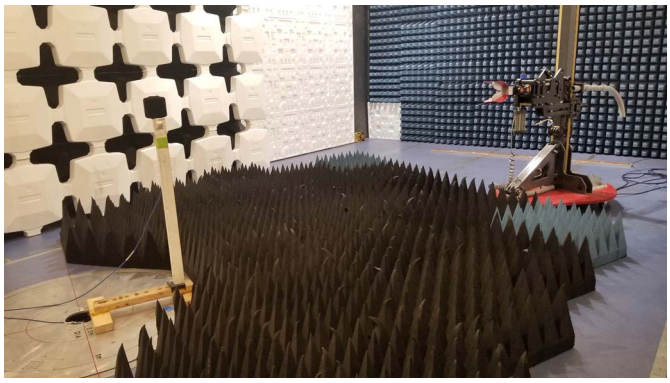

Fig. 4. Opposite view of test setup showing the offset biconical.

II. Theoretical Background and Development

Detailed development of mode filtering-based scattering suppression measurement and post-processing-based techniques is beyond the scope of this article and is instead left to the open literature, e.g., [9], with merely a summary being presented herein. Despite a wide range of scattering suppression methods existing, generalized mode filtering, and orthogonalization-based post-processing techniques have found great application since their inception [10] and initial use with spherical near-field antenna test systems [11]–[13]. These approaches mainly relied upon spherical-mode-based treatments requiring 2-D acquisitions. However, with the introduction of cylindrical mode-based analysis with first cylindrical near-field [14] and then far-field antenna measurement [8],

[15] implementations, scattering suppression became available for the case where only a single great-circle cut had been acquired. Although the mathematical treatments and requisite modal expansions may differ from implementation to implementation, the underlying principles and measurement procedures remain very consistent across the gamut and will now be explained.

An antenna is generally installed within a test range in such a way that it is displaced as little as possible during an acquisition. Range multi-path reflections disturb the fields illuminating the antenna under test (AUT), thus the purpose of this strategy is to guarantee the illuminating field changes minimally during the acquisition, and in so doing minimizing any resulting measurement error. However, this measurement technique intentionally displaces the AUT away from the center of rotation [7]–[9]. This significantly increases the differences in the illuminating field making range multipath effects far more pronounced than they would otherwise. It is exactly this greater differentiation that makes the identification and extraction of range multipath viable.

Clearly, displacing the AUT from the center of rotation will increase the effective electrical size of the AUT. From standard cylindrical near-field theory, we may calculate the angular sample spacing requirement using [9]

$$\Delta\theta = \frac{2\pi}{2(k_0\rho_0 + n_1) + 1}. \tag{1}$$

Here, n_1 is a positive integer that depends upon the accuracy required (e.g., $n_1 = 10$ [9]), k_0 is the free-space wavenumber, and ρ_0 is the maximum radial extent (MRE) which is a cylinder that is coaxial with the azimuth axis and that is large enough to circumscribe the majority of the current sources [9]. However, as only a single cut is required, the additional data will not typically affect the duration of the measurement providing the measurements are taken on the fly and the receiver is sufficiently fast to be able to acquire the data before the next sample point is encountered. From (1), we can rearrange to find the highest frequency that we can process before the data may become under-sampled

$$f_{\max} = \frac{c}{2\pi\rho_0}\left[\left(\frac{\pi}{\Delta\theta} - \frac{1}{2}\right) - n_1\right] \tag{2}$$

where c is the speed of light ($\sim 3 \times 10^8$ m/s). For the case of a measurement with a 0.5 m MRE, and $n_1 = 10$, at 1° angular sample spacing, the maximum frequency is 16.2 GHz, after which the quasi-far-field data will become under-sampled.

Traditionally, translating the test antenna in this way also has an impact on the far-field distance [9] as this can be expressed in terms of the MRE. Thus conventionally, increasing the MRE will similarly increase the required range length such that

$$R = \frac{2D^2}{\lambda} \approx \frac{2(2\rho_0)^2}{\lambda} = \frac{8\rho_0^2}{\lambda}. \tag{3}$$

An SVSWR measurement is typical performed with the RSA at 3 m distance away. Technically, this is not sufficient to satisfy the far-field criteria. In this case, however, we consider the antenna pattern collected in the measurement to be in a quasi-far-field (where the field largely follows the optical ray behavior, but both magnitude and phase are still affected by the finite distances [9]).

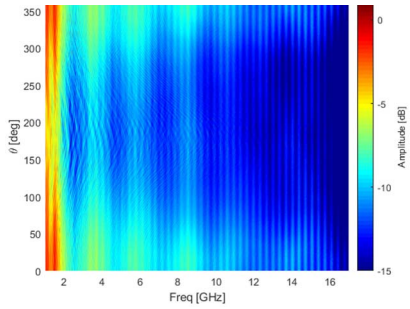

Fig. 5. Measured quasi far-field pattern data plotted as a false-color plot over frequency.

As we shall consider below, with the use of distance correction on both magnitude and phase, the requirement in (3) can be relaxed. Once a far-field cut has been taken, the AUT must be translated to the origin of the measurement coordinate system. In the true far-field, all the rays can be considered parallel, and the amplitude antenna pattern function is not dependent upon the distance. In such a case, only phase correction is needed, cf., [9]

$$\underline{E}_t(r \to \infty, \theta) = \underline{E}(r \to \infty, \theta) e^{jk_0 \cdot \underline{r}_m}. \tag{4}$$

Here, $\underline{r}_m$ is used to denote the displacement vector between the center of the measurement coordinate system and the center of the current sources, and θ is the rotation angle as shown in Fig. 1. Lastly, the measured far electric field is denoted by E, whilst the corresponding origin translated fields are E_t. In the true far-field, this expression is exact, however, in the case where the measurement range length is large but not infinitely large, a better correction can be obtained by incorporating the change in the finite range length making the amplitude and phase translation correction

$$\underline{E}_t(\theta) = \underline{E}(\theta) e^{jk_0\left(\sqrt{\left(R_0 - |\underline{r}_m|\cos\theta\right)^2 + \left(|\underline{r}_m|\sin\theta\right)^2} - R_0\right)} \times \frac{\sqrt{\left(R_0 - |\underline{r}_m|\cos\theta\right)^2 + \left(|\underline{r}_m|\sin\theta\right)^2}}{R_0}. \tag{5}$$

Referring to Fig. 1, R_0 denotes the distance between the RSA and the center of the azimuth rotation stage, which is serving as the origin of the measurement coordinate system and the symbol $\times$ denotes scalar multiplication. For a typical measurement, the correction applied in (5) is on the order of one or two decibels only. However, when using a vertically polarized bi-conical as the test antenna, the effect of the correction is evident, as can be seen, illustrated in Figs. 5 and 6 below.

This mathematical translation has the effect of reducing the number of mode coefficients, spherical or cylindrical, and so on, that are required to describe the equivalent far-field pattern [8], [9]. This is important since, by (3) as viewed traditionally, we are not in the true far-field, we are in the quasi-far-field. However, it can be argued that the data that

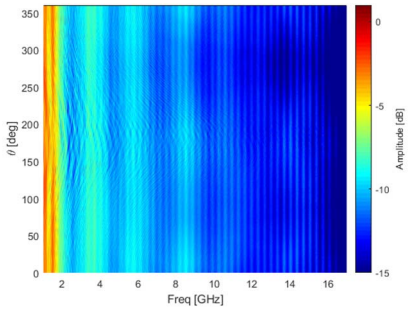

Fig. 6. Translated quasi far-field pattern data plotted as a false-color plot over frequency.

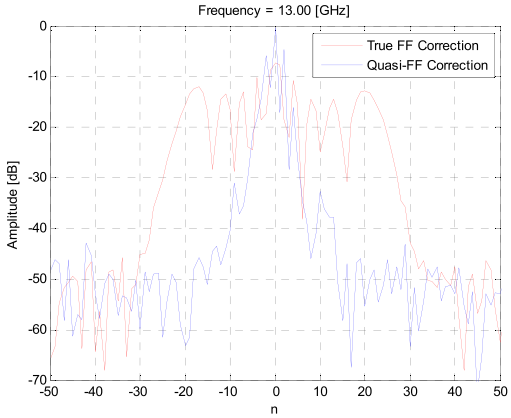

Fig. 7. Comparison of CMC spectra following antenna translation using true far-field correction, red, and quasi far-field correction blue.

we supply to the mode processing *have* been translated to the origin, using (5), and thus to a first order, with the finite range length amplitude and phase corrections applied, the mode processing is utilizing to a good approximation yielding reliable far-field data. Thus, the traditional application of the far-field criteria may consider the conceptual minimum MRE of the AUT [9] in the calculation of the far-field distance as opposed to using the conventional MRE. However, it is important to recognize that the translation operator is approximate in general and valid for electrically small antennas only. For example, it is rigorous for an infinitesimal dipole, but becomes progressively more unreliable as the electrical size of the test antenna increases for a given fixed, finitely large range length. Crucially, however, the test antenna that is employed within this testing regime is by design an electrically small, low directive antenna making it a viable candidate for this approach. This hypothesis will be further proven by an independent method, as will be shown in Section IV below.

The equivalent CMCs can be obtained from the compensated far-electric-fields using standard cylindrical theory [9]

$$B_n^1(\gamma) = -\frac{(-j)^{-n}}{4\pi k \sin\theta}\int_0^{2\pi} E_\varphi(r\to\infty,\theta,\varphi)e^{-jn\phi}d\phi \quad (6)$$

$$B_n^2(\gamma) = -j\frac{(-j)^{-n}}{4\pi k \sin\theta}\int_0^{2\pi} E_\theta(r\to\infty,\theta,\varphi)e^{-jn\phi}d\phi. \quad (7)$$

Here, ϕ represents a rotation about the vertical azimuthal axis (this is a more convenient coordinate system for our application; however, it does differ from what is commonly used in the development of the standard cylindrical near-field theory). For a fixed measurement radius and frequency, these B_n mode coefficients are complex numbers that do not vary with any of the scanning variables and conversely are functions of n the angular index, and γ the Fourier variable such that $-\infty \le n \le \infty$ and $-\infty \le \gamma \le \infty$. Here, as per the usual convention, the unimportant far-field spherical phase factor and inverse r term have been suppressed.

A comparison of the equivalent CMCs for the case, where the test antenna has been translated to the origin using the asymptotic far-field translation (4), cf., Fig. 5, and the modified ray-based quasi-far-field translation (5), cf., Fig. 6, can be seen in Fig. 7, where the axes have been adjusted to emphasize the AUT modes. From inspection of Fig. 7, it is evident that the CMCs are far more narrowly distributed about the 0th order mode for the case where the more accurate quasi far-field translation operator has been used than is the case for the ideal far-field translation. This results in far more effective filtering of the CMC spectra providing a more reliable chamber performance estimation than would otherwise be the case. It is worth noting that this operator is not limited to the EMC application being considered here but rather can be used with any far-field measurement, excluding of course measurements where the data were acquired using a compact antenna test range (CATR) where the AUT translation would result in the AUT passing outside the region of the pseudo plane wave [20]. Here, it is worth noting that these transforms and their inverse operations can be evaluated using the 1-D fast Fourier transform (FFT) which makes the processing algorithm very efficient in terms of computational effort. It is, however, worthwhile to use a mixed-radix FFT so as to be able to work with arrays that are not a power of two long, so as to be able to not zero-pad the data and therefore preserve the accuracy of the reconstructed mode-filtered far-field pattern cut at the edges of the sampling interval.

Strictly, (6) and (7) are only valid in the true far-field. However, providing the measurements are taken with a finite but sufficiently large range length that guarantees the far-field condition is satisfied [9], these integrals may be used with a high degree of confidence. Equally, probe pattern correction can be ignored since in the far-field the MRE cylinder only subtends a very small angular region as observed from the RSA [9]. That is, the RSA pattern is sufficiently constant across the test antenna that its effects may be ignored. Lastly, the highest order cylindrical mode that can be calculated from the far-field measured data is determined from [9]

$$n_{\text{Max}} = \text{ceil}\left(\frac{\pi}{|\Delta\phi|}\right). \quad (8)$$

From inspection of (6) and (7), the transverse electric (TE) and transverse magnetic (TM) CMCs are uncoupled from one another, and that the θ- and ϕ-polarized electric fields are also uncoupled from one another. This, therefore, allows this processing to be applied to only a *single* far electric field component. Dual polarized acquisitions are therefore not required in all instances offering the possibility of further reducing test times.

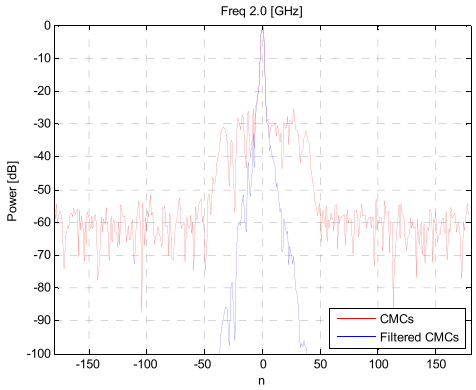

Fig. 8. CMCs plot before and after filtering at 2 GHz, where the chamber's performance is poorest.

When the CMCs for the now ideally positioned AUT have been recovered, any mode representing fields outside the ideal conceptual minimum MRE (r_t) can be filtered out, removing contributions that are not associated with the AUT [9]. Hence, because of standard cylindrical theory [9], it is possible to remove all higher-order modes without degrading the integrity of the underlying antenna pattern. Several different bandpass filter functions may be employed for this task, with a cosine squared windowing function constituting a good candidate in many applications [9].

As a full great-circle cut is acquired, in the absence of blockage, i.e., assuming the AUT support structure does not come between the AUT and RSA, this affords the experimentalist the possibility of determining the AUT offset. This can be done either in the time domain by comparing the difference in the time of arrival for the $\theta = 0°$ and $\theta = 180°$ positions, or by examining the phase change between the two positions. In either case, half the difference is the AUT offset radius. In many instances, it is easier and more accurate to determine the magnitude of the displacement in this way rather than by attempting to determine it directly, e.g., with a measure and so on. In this case, using inverse Fourier transform and viewing the time domain impulse responses for the front and back positions of the antennas, the time difference was determined to be 3.23 ns or equivalently 0.969 m, therefore making the AUT displacement 0.4845 m.

In effect then, the contributions in the CMC domain of the AUT and the scatterers are separated by the translation so that they interfere minimally with one another and are therefore orthogonalized [17]. As demonstrated computationally in [17], and experimentally in [9], it has been shown that the mathematical translation that is applied results in those modes associated with the AUT being shifted to lower order modes whereas those modes associated with scatterers are displaced toward higher-order modes with the amount of mode spectrum displacement being proportional to the magnitude of the physical shift. This is true for both the TE and TM mode sets, and making this technique effective on each field component and thus on both copolar and cross-polar data [9]. This is evident from the results shown in Figs. 12 and 13, where both vertical and horizontal SVSWR data show similar trends corresponding to the absorbers used in the chamber. Providing the displacement is as large as the maximum dimension of the antenna, and larger than three wavelengths for the case of electrically small radiators, reliable filtering is achieved. Gregson and Tian [17] present a purely CEM verification of the mode filtering technique, where the requirements for a successful application of the method are expounded. The inversion of (5) and (6) is then used to reconstruct the filtered far-field pattern [9]. A comparison of the measured, i.e., perturbed cut, and the filtered, i.e., reference cut, can be used to obtain the ripple in the measurement. The difference between the maximum and minimum ripple as a function of frequency is thus used to characterize the chamber. Results of this processing are presented and discussed in Sections III and IV.

III. Data Using Ray-Based Finite Range Translation

The experimental arrangement depicted in Fig. 1 and shown in Figs. 2 and 3 was used to acquire the amplitude data shown in Fig. 5 and accompanying phase data, not shown due to space constraints. The algorithm set out above in Section II was then used to compute the mode filtered great circle far-field pattern cut across the 1–18 GHz frequency band with 1601 frequency points. Fig. 8 contains a plot of the equivalent CMC spectrum for the 2 GHz case, which is a frequency that the chamber is known to perform less well due to the transition between the dielectric foams and the ferrite tiles used by the hybrid absorbers. Here, the reconstructed CMCs prior to filtering clearly show the effects of higher-order modes that are a consequence of chamber reflections. After translation by (5), the MRE is reduced to the size of the antenna; therefore, the number of modes needed to represent the antenna is limited to the lower orders, proportional to the now reduced MRE encompassing the centered antenna, instead of the antenna with an offset. At the same time, the modes from the reflections cannot be coherently translated by (5) because of the incoherent varying relationship between the antenna and the reflection points. The CMCs are filtered, using a cosine squared filter function, whereupon the mode filtered far-field pattern is computed. Fig. 9 contains the equivalent plot showing the measured great circle far-field azimuth pattern cut with and without mode filtering, which is denoted by the black and blue traces, respectively. The magenta trace is the difference plot which permits us to obtain a measure of the performance of the chamber at this specific frequency. In practice, this is accomplished by computing the maximum of the difference minus the minimum of the difference. This enables us to determine the SVSWR. Thus, in essence, we are looking at the difference between a scattering contaminated antenna measurement and a "clean" antenna measurement. Since the antenna pattern is the same in each case, the precise properties of its pattern can be seen to be suppressed when we compute the difference thereby reducing the sensitivity of this technique to the influence of the particular antenna being used, providing of course that the measurement is sufficiently sensitive.

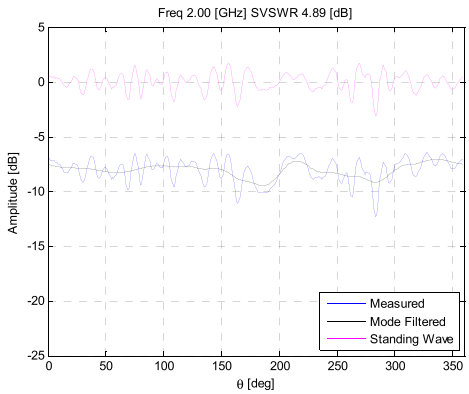

Fig. 9. Azimuth cut with and without processing at 2 GHz where the chamber performance is poorest.

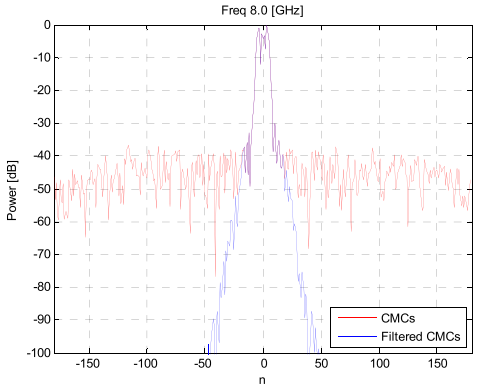

Fig. 10. CMCs plot before and after filtering at 8 GHz, where the chamber's performance is best.

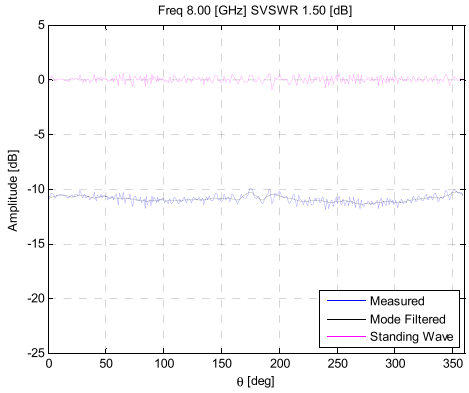

Fig. 11. Azimuth cut with and without processing at 8 GHz where the chamber performance is best.

It should be noted that the standard deviation of the ripple values can be calculated here, and instead of reporting the maximum difference as the SVSWR, results using a different statistical coverage factor can be reported, similar to the way time domain SVSWR is treated in ANSI C63.25.1 [16] in order to match the test severity of the CISPR SVSWR results.

Similarly, Figs. 10 and 11 are equivalent plots for the 8 GHz case, which is a frequency at which the chamber is known to perform well. The slightly broader AUT spectra is a natural consequence of a fixed MRE and an increase

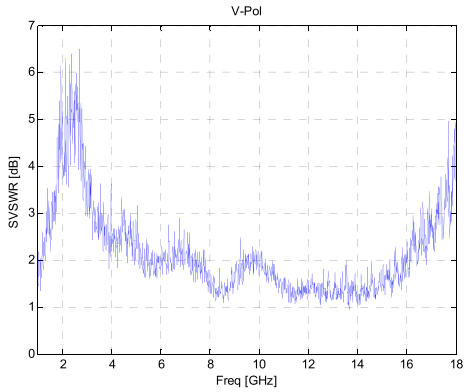

Fig. 12. SVSWR plot for V-pol measurement.

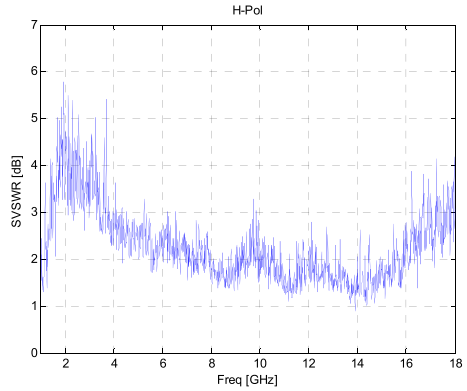

Fig. 13. SVSWR plot for H-pol (0°) measurement.

in frequency permitting a larger number of modes to be used to represent the same antenna as from the sampling theorem the maximum mode that is associated with the AUT is $n_{\max} = k_0 a$ where a is the MRE [9]. Thus, at each frequency, the mode windowing function is adjusted to take this into account. Here, by comparing the respective magenta traces in Figs. 9 and 11, we may evaluate the difference in the performance of the anechoic chamber at these two frequencies. Thus, by computing this site VSWR at each frequency it is possible to build up a measure of the chamber's performance across the 1–18 GHz band. This can be seen presented in Fig. 12 for the vertical polarization case, and Fig. 13 for one of the horizontal polarization cases. It was also noted the result was relatively insensitive to angular sample spacing with very similar SVSWR results being obtained when only half the number of angular samples were utilized by the processing.

To further validate the proposed method, the result shown in Fig. 12 is compared to the time domain SVSWR (TD SVSWR). The TD SVSWR method is described in ANSI C63.25.1 [16]. The broadband frequency response data at a specific test location are first inverse-transformed to the time domain. Fig. 14 shows the time domain response for the front test position (at $\theta = 0°$). The main peak occurs at ∼10 ns, which corresponds to the antenna-to-antenna distance of 3 m (the slight delay is due to the internal cable lengths of the antennas). Here, reflections within the chamber can

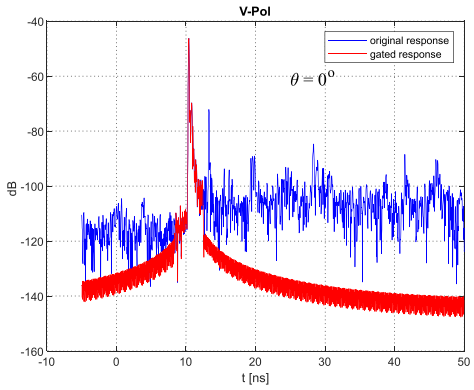

Fig. 14. Time domain response at the front edge of the QZ (F6 test point).

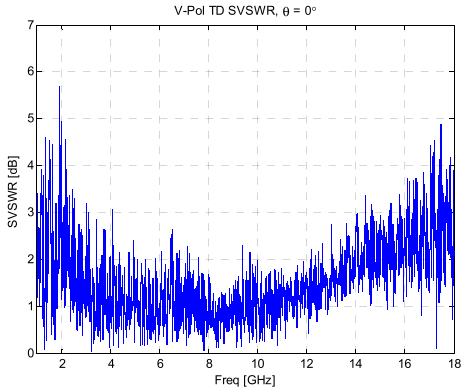

Fig. 15. SVSWR plot for V-pol measurement as computed using the time domain filtering method, cf., Fig. 12 above.

be observed at later times. A bandpass gate and a band-stop gate are then applied around the main peak, representing the responses of the unperturbed response and the response of the chamber reflections. These two time domain response curves are then transformed back to the frequency domain. The chamber reflection coefficient, $|\Gamma|$, is calculated by taking the ratio of the band-stop gated frequency response to the bandpass gated data. The SVSWR is then given by

$$\text{SVSWR} = \frac{1+|\Gamma|}{1-|\Gamma|}. \tag{9}$$

Fig. 15 shows the resulting TD SVSWR (vertical polarization and $\theta = 0°$). We do not expect to see a perfect correlation because the TD SVSWR data are for a single test position, whereas the mode filtered data (Fig. 11) are obtained from the *entire* circular cut. However, from observation, we can see that the overall trend of these data from these two independent methods agrees rather well, with both datasets showing the chamber performed worst near 2 GHz with deviations close to 6 dB and near 18 GHz with deviations close to 4 dB.

IV. Quasi-Far-Field to Far-Field Transform-Based Processing

In the analysis presented above, a finite range length correction was used to translate a quasi-far-field measurement of an electrically small antenna from the test position back to the origin of the measurement coordinate system so that the equivalent mode spectrum could be effectively computed, and thus filtered. The success of this approach, cf., (5) above, was largely predicated on the antenna being both electrically small and acquired in the quasi-far-field. However, these assumptions may not always hold true, or at the very least may require further verification before they can be relied upon more generally. Thus, the mandate for establishing an alternative, more general approach is clear. This section will initially present one such cylindrical mode-based transform before proceeding to utilize it, together with the aforementioned mode filtering technique, to obtain the SVSWR chamber qualification data where it will be compared against the results presented above.

The acquisition of an electrically small but single-axis offset antenna corresponds electromagnetically and conceptually to that of measuring an antenna that is very much larger in the translated axis than it is in the orthogonal axis [9]. Under these conditions, it has been shown that a cylindrical mode expansion based quasi-far-field to far-field transformation can be developed that allows measurements such as those considered herein to be corrected for finite range length effects providing the measurement distance satisfies the far-field condition for the smaller vertical dimension, i.e., height, of the antenna [18]. The derivation is predicated upon standard cylindrical near-field theory [9] with the cylindrical measurement being considered to tending toward the limiting case of a measurement comprising a single circular cut. In this treatment, probe pattern compensation is omitted on the basis that it has negligible effect in the vertical axis, as a result of the small-subtended angle of the antenna and the far-field range-length in this axis and, as at quasi-far-field distances in the orthogonal azimuth axis, such as those considered herein, probe directivity pattern effects are generally second-order perturbations that may be negated in many cases [18], [19]. Any effect on the far-field pattern is primarily on the main beam and the sidelobes have, generally, very small errors. Although this is in principle an approximation, in this case where the ratio of the range length to the minimum cylinder radius is 7, the rms dB difference level that this introduces for a low-directive RSA such as that used here will be very small and can be expected to be below -60 dB [19], which as can be seen above falls significantly below the pattern levels that are required by the SVSWR method considered herein. Thus, through the use of (9) and (12) in [18], it is possible to transform measured quasi-far-field data to the asymptotic far-field. Fig. 16 presents a false-color checkerboard plot of the transformed far-field pattern plotted as a function of angle and frequency, cf., Fig. 6 above. The effect of the quasi-far-field to true far-field transform can be seen, as before, by the increase in uniformity of the pattern as a function of angle, θ. It is important to note that at 16.2 GHz, the data become undersampled, as discussed previously (in Section II). This, therefore, yields unreliable far-field data starting at 16.2 GHz and affects results at this and all higher frequencies. The effect that this has on the SVSWR data will be examined further below.

Once a far-field cut has been obtained, as was the case with the processing presented above, the AUT must be mathematically translated to the origin of the measurement

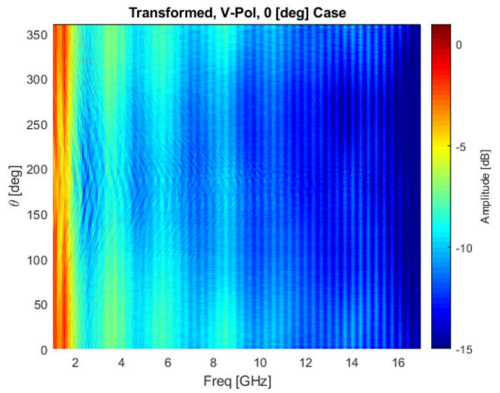

Fig. 16. Transformed far-field pattern data plotted as a false-color plot over frequency.

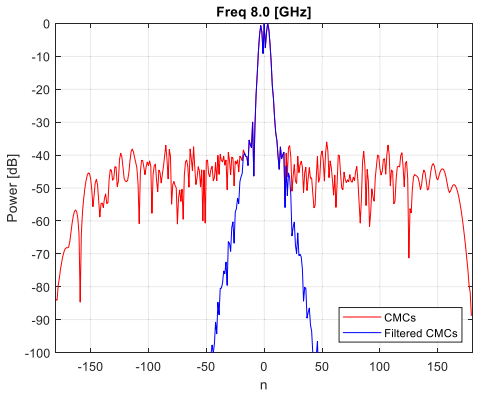

Fig. 17. CMCs plot before and after filtering at 8 GHz, where the chamber's performance is best.

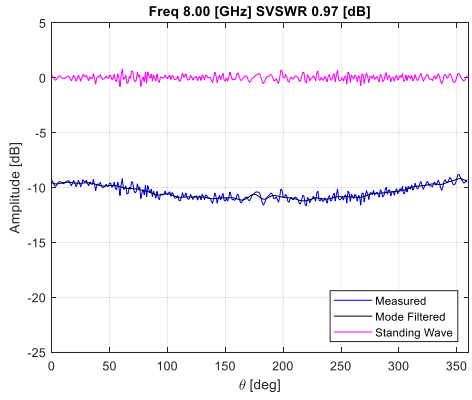

Fig. 18. Azimuth cut with and without processing where the chamber performance is best.

coordinate system. Here, however, we may accomplish this rigorously using (4) which is a pure phase compensation [9]. The remainder of the processing is identical to that which was presented and employed within Section III. By way of a comparison with the previous processing, Fig. 17 contains a plot of the equivalent CMC spectrum for the 8 GHz case, with Fig. 18 presenting the equivalent plot showing the measured great circle far-field azimuth pattern cut with and without mode filtering. As before, these are denoted by the blue and

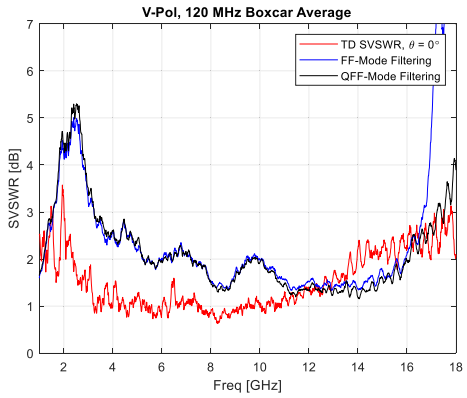

Fig. 19. Moving average SVSWR plot for V-pol measurement.

black traces, respectively, with the magenta trace representing the difference plot. From inspection of these plots and by comparing them with Figs. 10 and 11, respectively, it can be seen that the more general processing has produced very similar results to the approximate method presented above. As before, as the antenna pattern is the same in each case. The precise properties of its pattern can be seen to be suppressed, including any remaining probe effects, when we compute the difference thereby reducing the sensitivity of this technique to the influence of the particular antenna being used.

As before, the SVSWR can now be computed from the processed pattern data and plotted as a function of frequency. This was done, however, in order that the underlying trend could be more easily interpreted, a running average was applied to the SVSWR data. This involved taking the mean average over a sliding 120 MHz wide frequency band and is a post-processing technique that is in common with the convention adopted by the ANSI C63.25.1 [16] standard. These results can be seen presented in Fig. 19. Here, the red trace denotes the 120 MHz boxcar (i.e., running) averaged time-domain SVSWR result, the blue trace denotes the equivalent transformed SVSWR result and the black trace denotes the quasi-far-field processed SVSWR result, i.e., the result presented within the preceding section.

From inspection of Fig. 19, it is clear that new far-field mode filtered result is in very encouraging agreement with the prior obtained quasi-far-field mode filtered result for frequencies below 16 GHz. As noted above, the transformed data are under-sampled at frequencies above 16 GHz, and the significant rise in the SVSWR level seen here is a direct consequence of a failure to satisfy this requirement. As expected, the TD SVSWR data are generally smaller, because unlike the mode filtered methods, the time domain data are derived based on a single position.

V. Summary and Conclusion

In this article, a novel SVSWR measurement method for evaluating EMC chambers is proposed based on placing an omni-directional antenna at an offset position, i.e., the outer edge of the turntable, and collecting several 1-D pattern cuts. CMC filtering is applied to separate the antenna response from the chamber reflections based on the cylindrical mode filtering

algorithm [9], [15]. Two techniques were explored for translating the vector pattern data back to the rotation center, through a finite range distance ray-based translation, or through a more general quasi-far-field to true far-field transformation and then rigorous far-field antenna translation. The two techniques are shown to yield equivalent results, giving confidence for the validity of both. A mode filter is then applied after the coordinate translation. The difference between the uncorrected pattern and the mode filtered pattern is used to derive the SVSWR. The proposed method overcomes the difficulty associated with under-sampling the standing wave pattern in the traditional CISPR SVSWR technique. It is easy to implement using existing turntable within an EMC chamber, with no other special positioning equipment needed. Three great circle pattern cuts with different antenna orientations are proposed, which can fully quantify the chamber SVSWR, and therefore the measurement data can be acquired with minimal test time. There is also a distinct advantage over the TD SVSWR method specified in the ANSI C63.25.1 [16] standards—the proposed method does *not* rely on using broadband antennas, and works equally well for antennas with long ring-down times, where a time-domain method may have difficulties separating main responses from chamber reflections.

REFERENCES

[1] *Specification for Radio Disturbance and Immunity Measuring Apparatus and Methods—Part 1-4: Radio Disturbance and Immunity Measuring Apparatus—Antennas and Test Sites for Radiated Disturbance Measurements*, Standard CISPR/CIS/A, CISPR 16-1-4:2019, Jan. 2019.

[2] M. J. Windler, "Site qualification above 1 GHz and SVSWR systemic errors," in *Proc. Asia–Pacific Int. Symp. Electromagn. Compat.*, 2010, pp. 565–568.

[3] Z. Chen, "Uncertainties in SVSWR and a proposal for improvement using vector response measurements," in *Proc. Int. Symp. Electromagn. Compat.*, Tokyo, Japan, 2014, pp. 274–277.

[4] T. Tosaka and Y. Yamanaka, "Evaluation of uncertainty in electromagnetic disturbance measurement in the 1–18 GHz range," in *Proc. 30th URSI Gen. Assem. Sci. Symp.*, Aug. 2011, pp. 1–4.

[5] Z. Chen, "A preview of draft ANSI C63.25 time domain site VSWR method," in *Proc. 10th Eur. Conf. Antennas Propag. (EuCAP)*, Apr. 2016, pp. 1–4.

[6] C. Culotta-López, Z. Chen, T. M. Gemmer, and D. Heberling, "Validation of electromagnetic compatibility chambers with a spherical wave expansion approach," in *Proc. Antenna Meas. Techn. Assoc. Symp. (AMTA)*, 2019, pp. 1–4, doi: 10.23919/AMTAP.2019.8906406.

[7] Z. Chen and S. Gregson, "Examination of EMC chamber qualification methodology for applications above 1 GHz using frequency domain mode filtering," in *Proc. Antenna Meas. Techn. Assoc. Symp. (AMTA)*, 2020, pp. 1–6.

[8] S. F. Gregson, J. Dupuy, C. G. Parini, A. C. Newell, and G. E. Hindman, "Application of mathematical absorber reflection suppression to far-field antenna measurements," in *Proc. Loughborough Antennas Propag. Conf.*, 2011, pp. 1–4, doi: 10.1109/LAPC.2011.6114016.

[9] C. G. Parini, S. F. Gregson, J. McCormick, and D. J. van Rensburg, *Theory and Practice of Modern Antenna Range Measurements*. Edison, NJ, USA: IET, 2014.

[10] O. M. Bucci, G. D'Elia, and M. D. Migliore, "A general and effective clutter filtering strategy in near-field antenna measurements," *IEE Proc.-Microw., Antennas Propag.*, vol. 151, no. 3, p. 227, Jun. 2004.

[11] G. E. Hindman and A. C. Newell, "Reflection Suppression in a large spherical near-field range," in *Proc. Antenna Meas. Techn. Assoc. Symp. (AMTA)*, 2005, pp. 270–275.

[12] G. E. Hindman and A. C. Newell, "Reflection suppression to improve anechoic chamber performance," in *Proc. AMTA Eur. Symp.*, Munich, Germany, May 2006, pp. 297–302.

[13] D. W. Hess, "The IsoFilter technique: Isolating an individual radiator from spherical near-field data measured in a contaminated environment," in *Proc. 2nd Eur. Conf. Antennas Propag. (EuCAP)*, 2007, pp. 1–6.

[14] S. F. Gregson, A. C. Newell, and G. E. Hindman, "Reflection suppression in cylindrical near-field antenna measurement systems—Cylindrical MARS," in *Proc. Antenna Meas. Techn. Assoc. Symp. (AMTA)*, 2009, pp. 1–7.

[15] S. F. Gregson, J. Dupuy, C. G. Parini, A. C. Newell, and G. E. Hindman, "Application of mathematical absorber reflection suppression to far-field antenna testing," in *Proc. Loughborough Antennas Propag. Conf.*, 2011, pp. 1–4, doi: 10.1109/LAPC.2011.6114016.

[16] *American National Standard Validation Methods for Radiated Emission Test Sites, 1 GHz to 18 GHz*, document ANSI C63.25.1-2018, 2019.

[17] S. F. Gregson and Z. Tian, "Verification of generalized far-field mode filtering based reflection suppression through computational electromagnetic simulation," in *Proc. IEEE Int. Symp. Antennas Propag. North Amer. Radio Sci. Meeting*, Montreal, QC, Canada, Jul. 2020, pp. 5–10.

[18] X. Li, G. Wei, L. Yang, and B. Liao, "Fast determination of single-cut far-field pattern of base station antenna at a quasi-far-field distance," *IEEE Trans. Antennas Propag.*, vol. 68, no. 5, pp. 3989–3996, May 2020.

[19] A. C. Newell and S. F. Gregson, "Estimating the effect of higher order azimuthal modes in spherical near-field probe correction," in *Proc. 8th Eur. Conf. Antennas Propag. (EuCAP)*, 2014, pp. 2486–2490, doi: 10.1109/EuCAP.2014.6902323.

[20] S. F. Gregson, C. G. Parini, and S. Pivnenko, "Small antenna testing in a compact antenna test range," in *Proc. Antenna Meas. Techn. Assoc. Symp. (AMTA)*, San Diego, CA, USA, Oct. 2019.

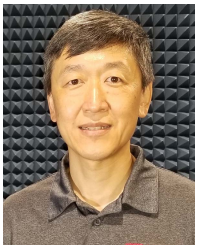

Zhong Chen (Member, IEEE) received the M.S.E.E. degree in electromagnetics from The Ohio State University, Columbus, OH, USA, in 1996.

He is the Director of Radio Frequency (RF) Engineering at ETS-Lindgren, Cedar Park, TX, USA. He has over 25 years of experience in RF testing, anechoic chamber design, as well as antenna and electromagnetic compatibility (EMC) field probe design and measurements. His research interests include measurement uncertainty, time domain measurements, and development of novel RF absorber materials.

Mr. Chen is currently serving as a Board Member for the Antenna Measurement Techniques Association (AMTA). He is the Chairman of Subcommittee 1 of ANSI ASC C63 which is responsible for EMC antenna calibration and test site validation standards. He is the Chairman of the IEEE Standard 1309 committee responsible for developing calibration standards for field probes and IEEE Standard 1128 for absorber measurements. He served as a Distinguished Lecturer for the IEEE EMC Society.

Stuart F. Gregson received the B.Sc. degree in physics and the M.Sc. degree in microwave solid state physics from the University of Portsmouth, Portsmouth, U.K., in 1994 and 1995, respectively, and the Ph.D. degree from Queen Mary University of London, London, U.K., in 2003, with a focus on near-field antenna measurements and statistical pattern recognition as his main subject areas.

He has in excess of 25 years of experience working in the space, aerospace, and communications sectors. He is the Director of Operations and Research at Next Phase Measurements, Garden Grove, CA, USA, and an Honorary Visiting Professor with the School of Electronic Engineering and Computer Science, Queen Mary University of London. He has developed special experience with near-field antenna measurements, finite array mutual coupling, computational electromagnetics, installed antenna and radome performance prediction, compact antenna test range design and simulation, electromagnetic scattering, and 5G over-the-air (OTA) measurements. He has published numerous peer-reviewed research papers on these topics regularly contributing to and organizing industrial courses on these subject areas. At the end of 2007, he was the lead author of the research text *Principles of Planar Near-Field Antenna Measurements*, and in 2014, he has coauthored a second text *Theory and Practice of Modern Antenna Range Measurements* (second edition).

Dr. Gregson is a fellow of the Antenna Measurement Techniques Association, the Institution of Engineering and Technology, and the Institute of Physics. He is also a Chartered Engineer and Physicist. In 2018, he was elected to the AMTA Board of Directors, where he served first as a Treasurer and currently as the Vice President.